Materials Chemistry and Physics 138 (2013) 581–592

Contents lists available at SciVerse ScienceDirect

Materials Chemistry and Physics

journal homepage: www.elsevier.com/locate/matchemphys

On-line phase transitions of bulk and nanocrystalline $La_{1-x}Pb_xMnO_3$ ($x = 0.3$, 0.4, and 0.5) perovskite manganite materials using ultrasonic measurements

K. Sakthipandi, V. Rajendran*

Centre for Nano Science and Technology, K S Rangasamy College of Technology, Tiruchengode 637215, Tamil Nadu, India

HIGHLIGHTS

- Exploring the nanostructured perovskite through observed anomalous at T_C.
- A sharp FM–PM transition for bulk $La_{1-x}Pb_xMnO_3$ perovskite samples.
- The diffused FM–PM transition for nano $La_{1-x}Pb_xMnO_3$ perovskite samples.

ARTICLE INFO

Article history:
Received 4 October 2012
Received in revised form
4 December 2012
Accepted 10 December 2012

Keywords:
A. Magnetic materials
C. Ultrasonic measurements
D. Phase transitions
D. Elastic properties

ABSTRACT

Bulk and nanostructured $La_{1-x}Pb_xMnO_3$ perovskite manganite samples for different Pb contents ($x = 0.30$, 0.40 and 0.50) were synthesised using solid-state reaction and sonochemical methods, respectively. XRD, FTIR, SEM, EDAX, BET and TEM studies were carried out to characterise the prepared bulk and nanosamples. The XRD characterization studies confirmed that the prepared bulk and nano perovskite manganite samples were crystalline in nature. The SEM and TEM studies revealed that the particle sizes of bulk perovskite samples is in the range of 0.75–85 μm, whereas it ranges from 50 to 90 nm in the case of nano perovskite samples. Further, it has been confirmed that there is an increase in particle size with an increase in Pb content both in bulk and nano perovskite samples. In addition, ultrasonic velocities and attenuations of bulk and nanosamples were measured using the on-line ultrasonic through transmission method. The temperature-dependent ultrasonic parameters showed an interesting anomaly in both bulk and nano perovskite samples. The observed marked softening and hardening in sound velocities and attenuation were related to ferromagnetic to paramagnetic phase transition temperature (T_C). In nano perovskites samples, the existence of diffused phase transition took place at a lower temperature compared with the corresponding bulk samples. The observed broad ferromagnetic (FM)–paramagnetic (PM) transition in nano perovskites confirms the absence of sharp transition, which is attributed to the coexistence of orbitally, ordered and disordered phases. The spin–phonon and electron–phonon couplings are known to exist because of single ion magnetostriction and dynamic Jahn–Teller effect, respectively, are evidenced by the observed anomalies in both velocities and attenuations.

1. Introduction

In recent years, the $La_{1-x}A_xMnO_3$ (where A is a divalent element like Ca, Sr, Pb, Na, and Rb) perovskite structure has attracted attention because of its interesting electrical and magnetic properties [1–6]. The doping of divalent ions instead of La in a $LaMnO_3$ insulator leads to an interesting behaviour in $La_{1-x}A_xMnO_3$ perovskites [4]. Doped manganites exhibit two types of transitions: electrical transition from the insulator to metal transition (T_P) accompanied by magnetic transition from paramagnetic to ferromagnetic transition (T_C). Generally, colossal magnetoresistance (CMR) is regarded as the most important parameter to be considered as a function of temperature; it takes the maximum value near the Curie temperature T_C [3,4]. However, a large magnetoresistance (MR) value is often obtained in a large magnetic field (up to several Tesla) and at low temperature; these conditions severely limit its applications [5–7]. To realize its applications in many fields, the

* Corresponding author. Tel.: +91 4288 274741/4/274880; fax: +91 4288 274880 (Direct)/274745.
E-mail address: veerajendran@gmail.com (V. Rajendran).

0254-0584/$ – see front matter © 2012 Elsevier B.V. All rights reserved.
http://dx.doi.org/10.1016/j.matchemphys.2012.12.023

field sensitivity and working temperature of perovskite manganites have to be improved [8].

The double-exchange mechanism can be considered as the basis for the explanation of the paramagnetic to ferromagnetic transition and the associated CMR effect. Similarly, the Jahn–Teller effect and the strong electron–phonon interactions are used to explore the transition in perovskites [4,5]. The double-exchange (DE) interaction between pairs of Mn^{3+} and Mn^{4+} ions through an oxygen atom is responsible for the ferromagnetic and metallic properties of these manganese oxides [9]. Therefore, knowledge of the structural properties of perovskites, like surface spin, structure disorders, half-metallicity, and their possible influence on magnetism, is an essential requirement [10,11] while studying the use of manganite oxides for a wide range of applications.

Extensive work on the role of pressure and temperature, both external and internal (chemical), on the physical and magnetic properties of different forms of perovskites like single crystals [12,13], bulk polycrystalline materials [14,15], and thin films [16,17] has been carried out. Recently, efforts were made to synthesise and characterise the properties of nanostructured perovskites in different forms, such as nanoparticles [18,19], nanocubes [20], nanorods [21], nanobelts [22], nanosheets [23], nanowires [24], and nanotubes [25], with a view to explore the distinctive physical properties for potential application in, for example, nanodevices [26]. Nanostructured manganites with large grain boundaries (GBs) are known to exhibit pronounced low field magnetoresistance properties [27]. Nanostructured perovskites exhibit fascinating size-dependent optical, electronic, magnetic, thermal, mechanical, and chemical properties, which are distinct from those of their corresponding bulk perovskites [21,24–27]. The nanostructured LPMO shows promising applications, such as in piezoelectric transducers and actuators, ultrasonic devices, fuel cells, infrared devices, magnetic sensors, magnetic reading heads for memory devices, and non-volatility memory devices [28–30]. $La_{1-x}Pb_xMnO_3$ (LPMO) manganite shows a ferromagnetic metallic (FMM) phase at room temperature along with large magnetoresistance. Similarly, LPMO manganites in their bulk phase have shown potential for a wide range of applications such as in magnetic field sensors, hard disk read heads, and microwave active components because of their unique physico-chemical and large giant magnetoresistance (GMR) properties [30–33].

The structural and physical properties of LPMO perovskites have been studied through different techniques like ac susceptibility, specific heat, and electrical resistivity measurements [28,30,31]. Among these studies, characterisation of LPMO perovskites through ultrasonic nondestructive testing [34–37] is a novel and promising technique by which to examine the structural/phase transitions on-line and correlate the differences between FM and PM phase physical properties [33]. A basic understanding of ultrasonic waves and knowledge of the availability of a wide range of frequencies and more sophisticated instruments make the measured ultrasonic velocities and attenuations highly sensitive parameters for material evaluation [34–36]. Thus, the interactions of ultrasonic waves and the coupling in perovskite manganite materials between the structural, spin orbital, and strain lead to corresponding changes in lattice. The lattice degrees of freedom are directly linked to the measured velocities and attenuations, which in turn are used to explore the structural and phase transition changes in materials [37].

Therefore, in the present study, series of bulk and nanocrystalline $La_{1-x}Pb_xMnO_3$ perovskite manganite particles for three different compositions (0.3, 0.4, and 0.5) were prepared using solid-state reaction and sonochemical methods. The structural and compositional purity, along with the morphology and properties of prepared samples, have been characterised using different techniques. A systematic study on both bulk and nano LPMO perovskites samples has been conducted using on-line ultrasonic studies as a function of temperature in order to gain insight into the behaviour of transition and the microscopic origin of the CMR effect.

2. Materials and methods

2.1. Preparation of samples

Bulk phase $La_{0.7}Pb_{0.3}MnO_3$, $La_{0.6}Pb_{0.4}MnO_3$, and $La_{0.5}Pb_{0.5}MnO_3$ samples (hereafter termed BLPMO3, BLPMO4, and BLPMO5, respectively) were prepared using the solid-state reaction technique. The chemicals used were of GR/AR grade without any further purification. Required quantities of lanthanum nitrate (99.999%, Sigma Aldrich), manganese carbonate (99.9%, Sigma Aldrich), and lead nitrate (99.0%, Himedia GR) powders were used as starting materials. These starting materials in their stoichiometric ratios were mixed in an agate mortar. The grainy powder thus obtained was preheated at 873 K in air for 4 h with intermediate grinding three times for better crystallisation. The obtained fine mixture was used to acquire the bulk perovskite manganite material. The nano structured perovskite $La_{0.7}Pb_{0.3}MnO_3$, $La_{0.6}Pb_{0.4}MnO_3$, and $La_{0.5}Pb_{0.5}MnO_3$ samples (hereafter termed NLPMO3, NLPMO4, and NLPMO5, respectively) were prepared by the sonochemical method with a high-intensity titanium horn (Sonics, USA) operated at a frequency of 20 kHz using a rated power output of 240 W. The insoluble manganese carbonate was converted into soluble nitrate by sonication in dilute nitric acid for 20 min. Lanthanum and calcium nitrate salt solutions were added to the manganese solution during the sonication process at a constant temperature of 353 K. The solution was allowed to dry in a hot air oven at 403 K for 24 h by adjusting the pH value of the solution to ~7. The residue formed was collected and then calcined in air at 873 K for 2 h. Both bulk and nano calcined powders were pressed into a pellet separately and sintered at 1273 K for 12 h in atmospheric air.

2.2. X-ray diffractometry

X-ray diffraction (XRD) patterns of the prepared bulk and nano LPMO samples were determined using a powder X-ray diffractometer (X'Pert Pro, Analytical, Netherland) at a scan range of 10–80° at a scanning rate of $1^\circ\ min^{-1}$ using a monochromatised CuK_α radiation source operated at 40 kV and 30 mA. The relative atomic position of atoms and the crystallite size (D_{xRD}) of BLPMO and NLPMO perovskite samples were obtained by knowing the full-width at half-maximum ($\beta_{1/2}$), Millers indices (hkl), and angle of diffraction (θ) of XRD Bragg's peaks using Rietveled and Scherrer's equations [38,39].

2.3. Density

The density of bulk and nano LPMO sintered pellets was measured by the liquid displacement method (the Archimedes method) using CCl_4 as a buoyant. The weights of the sample in air and buoyant (W_a and W_b, respectively) were measured using a digital balance (Sartorius, Germany). The density of the sample [34–36] was

$$\rho = \frac{W_a}{W_a - W_b}\rho_b \quad (1)$$

where ρ_b is the density of the buoyant sample. The measurement was taken ten times with different sizes of pellets to obtain the precise density value for each composition. The mean value of

density was taken as the density of the sample. The percentage error in the measurement of density was ±0.05.

2.4. Fourier transformation infrared spectroscopy

To interpret the different vibrational modes, involving pairs/groups of atoms and the functional groups existing in the prepared bulk and nano LPMO perovskite samples, Fourier transformation infrared (FTIR) spectra were recorded using a spectrometer (Spectrum 100, PerkinElmer, USA). The spectra were recorded in the wavenumber range from 4000 to 400 cm^{-1} at room temperature in different reflectance modes at a resolution of 1 cm^{-1}. The samples used for the measurements were obtained using the KBr pellet method. The KBr discs were made by pressing the mixture, which contained 10 mg of samples with 100 mg of KBr, at a pressure of 125 kg cm^{-2}.

2.5. Microscopy

The microstructure, morphology, and compositions of bulk and nano LPMO were analysed using SEM/EDX images obtained using a scanning electron microscope (JEOL, JED 2300, Japan) integrated with the energy dispersive analysis of an X-ray (EDX) spectrometer with a magnification from 5× to 3,00,000×. The spectrometer was operated at an accelerating voltage of 30 kV. A transmission electron microscope (TEM, Philips, CM 200, USA) was used to obtain substructural information and particle size of the prepared samples by recording TEM images. The samples for TEM studies were prepared ultrasonically by dispersing the samples in methanol and allowing a drop of this solution to dry on a carbon-coated copper grid.

2.6. BET surface area

The nitrogen absorption isotherm was used to measure the surface area (S_{BET}) of BLPMO and NLPMO samples using a Brunauer–Emmett–Teller (BET) surface area analyser (Autosorb-1, Quantachrome, USA). To avoid any thermally induced changes on the surface of the particles, the N_2 adsorption–desorption BET measurements were taken at liquid nitrogen temperature. Before taking the BET measurements, the samples were degassed under vacuum at 568 K for 3 h to remove physically absorbed gas molecules and moisture. The equivalent spherical diameters (D_{BET}) of BLPMO and NLPMO perovskite samples were obtained from the measured surface area and density using the standard equation [40].

2.7. Ultrasonic velocities and attenuation

An indigenously designed experimental set-up available in the authors' laboratory [34,35] was used to measure the ultrasonic velocities (U_L and U_S) and attenuation (α_L and α_S) of both BLPMO and NLPMO samples. A high-power ultrasonic Pulsar Receiver (Olympus NDT, 5900 PR, USA) and a high-frequency (1 GHz) digital storage oscilloscope (DSO) (Lecroy, Wave Runner 104 MXi, USA) were used for the transmission and reception of ultrasonic sound using a standard transmission technique. The longitudinal and shear ultrasonic waves were generated at a fundamental frequency of 5 MHz using X-cut or Y-cut transducers, respectively. Before obtaining the ultrasonic measurement, both surfaces of the sintered samples were first cleaned by polishing and then cleaned with isopropanol to remove moisture from the surface. The ultrasonic velocities and attenuation measurements were taken on bulk and nano LPMO perovskite samples as a function of temperature from 300 to 400 K. The temperature of the sampled region was controlled using a Eurotherm temperature controller (2604, Eurotherm, USA) with a heating rate of 0.5 K min^{-1}. Measurements were taken from 300 to 1200 K using the procedure as discussed in our earlier studies [36,37]. The standard procedure was used for the couplant correction on the measured velocities and attenuation [35,41]. The measured density (ρ) and longitudinal (U_L) and shear (U_S) velocities were used to obtain the longitudinal, shear, bulk, Young's modulus, Possion's ratio, and the first derivative of ultrasonic velocity for both BLPMO and NLPMO samples using standard formulae [34–36].

3. Results and discussion

The XRD pattern of bulk and nano LPMO perovskites is shown in Fig. 1. The observed diffraction peaks in the XRD pattern of bulk and nano LPMO samples were used to explore the crystalline nature of the prepared samples. The observed XRD peaks of bulk LPMO perovskite manganite samples were indexed and well matched with the triclinic ($x = 0.3$), rhombohedral ($x = 0.4$), and cubic ($x = 0.5$) phases (JCPDS files Nos. 85-1788, 4-095-1256 and 65-3287) as reported elsewhere [31]. It is interesting to note that the crystal symmetry changed from triclinic ($x = 0.3$) to cubic ($x = 0.5$) with an increase in Pb content in BLPMO perovskite manganite samples, whereas the diffracted peaks of all nanostructured LPMO perovskite manganite materials matched well with the rhombohedral structure (JCPDS files No. 4-095-1256). Further, the broad XRD peaks of nano LPMO perovskite samples shifted towards a lower diffracted angle when compared with the corresponding bulk perovskite samples. For example, the triclinic peak of the (110) plane of BLPMO3 and the rhombohedral peaks of the (011) plane of NLPMO3 were located at $33.425 \pm 0.05^\circ$ and $33.375 \pm 0.05^\circ$, respectively. The shift in peak position may have been due to the smaller particle sizes of nano LPMO perovskite samples. The average crystallite sizes (D_{xRD}) were obtained from the full-width at half-maximum (FWHM) ($\beta_{1/2}$) of the diffracted peaks using Scherrer's equation, i.e., $D_{xRD} = 0.94\lambda/(\beta_{1/2}\cos\theta)$, where λ is the X-ray wavelength and θ is the diffraction angle. The crystallite sizes of the particles were 0.34, 0.41, and 0.49 μm for BLPMO3, BLPMO4, and BLPMO5, respectively, whereas the sizes were 37, 43, and 54 nm for the nanosamples NLPMO3, NLPMO4, and NLPMO5, respectively.

The Mn–O–Mn bond angles and the Mn–O bond length for bulk and nano LPMO perovskites obtained using Rietveld's profile-fitting technique [38,39] are given in Table 1. The single position for the oxygen state in rhombohedral and cubical structures and three independent positions for oxygen states in the triclinic structure are noted separately in Table 1. It is evident from Table 1 that the Mn–O bond length decreases with an increase in Pb content both in bulk and nano LPMO perovskites. The decrease in Mn–O bond length clearly indicates that an increase in Pb content in LPMO perovskites leads to tight bonding between the Mn and O atoms [31]. The Mn–O bond length is one of the essential parameters in the MnO_6 octahedral of perovskites samples and it influences the structural and physical properties of the perovskites [42]. Further, the decrease in Mn–O bond length confirms that the lattice constant and volume of unit cells decrease with an increase in Pb content in LPMO perovskite manganite samples [31]. The Mn–O–Mn bond length for nanostructured perovskite samples is higher than that for the corresponding bulk LPMO perovskite samples [43]. It is evident that the bonding between Mn and O atoms is less and weak in nano LPMO perovskite compared with bulk perovskite samples. Significant change in bond length between Mn and O atoms was observed during the transition from bulk to nano perovskite samples [34]. Thus, the structural properties of nano perovskite samples are distinguished from those of their corresponding bulk perovskites [35]. Further, it can be observed from

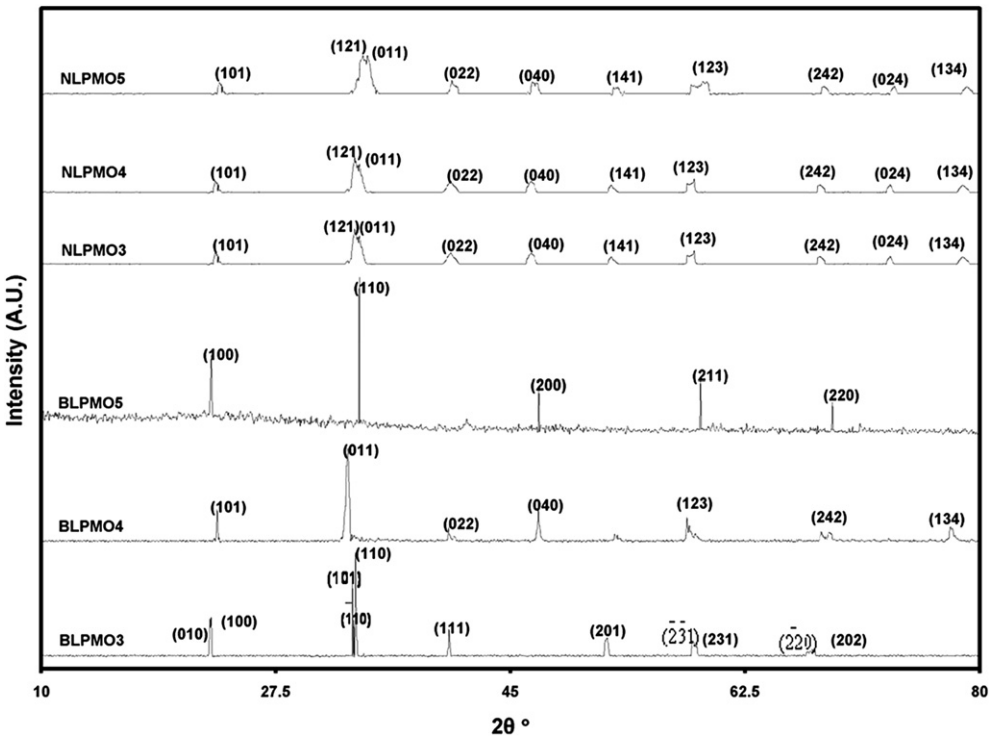

Fig. 1. XRD pattern of bulk $La_{0.7}Pb_{0.3}MnO_3$ (BLPMO3), bulk $La_{0.6}Pb_{0.4}MnO_3$ (BLPMO4), bulk $La_{0.7}Pb_{0.3}MnO_3$ (BLPMO5), nano $La_{0.7}Pb_{0.3}MnO_3$ (NLPMO3), nano $La_{0.6}Pb_{0.4}MnO_3$ (NLPMO4) and nano $La_{0.7}Pb_{0.3}MnO_3$ (NLPMO5) perovskite samples.

Table 1 that the Mn–O bond length decreases with an increase in grain size of LPMO perovskites. The decrease in Mn–O bond length in nano LPMO perovskites leads to a reduction in the overlap between the neighbouring orbits of Mn ions and the adjacent O ions [41,43]. Therefore, the double-exchange interactions between Mn^{3+} and Mn^{4+} ions via O^{2-} become very weak in nano perovskite samples than in the corresponding LPMO perovskite samples. Hence, the transition temperature of nano LPMO perovskites is lower than that of the corresponding bulk sample.

Fig. 2 shows the EDX spectra of both bulk and nano LPMO perovskite samples. It is clear from the EDX spectra that these samples are composed of elements La, Pb, Mn, and O atoms. The atomic ratio of the constituent elements obtained from the EDX pattern is given in Table 2. The atomic ratios of La, Pb, Mn, and O atoms are almost in close agreement with those of the nominal composition of the starting composition of bulk and nano perovskites. Further, the absence of emission lines present in the spectra confirms the absence of impurities both in bulk and nano perovskite samples. The observed FTIR spectra of bulk and nano perovskite samples are shown in Fig. 3. The observed broad band at 3400 cm^{-1} can be attributed to the O–H stretching vibration of water molecules [44,45]. The intense band observed at 1630 cm^{-1} corresponds to the H–O–H bending mode characteristic of water molecules [35,44]. Further, the observed broad peak in the low wavenumber range, i.e., 450–600 cm^{-1}, is ascribed to Mn–O bonds because of the Jahn–Teller effect (JT) in the prepared perovskite samples [35,44,45]. The assignment of functional groups from the FTIR spectra is given in Table 3, along with their corresponding wavenumber.

The surface area values for the bulk samples were 2.96, 2.37, and 2.34 $m^2\,g^{-1}$, respectively, for BLPMO3, BLPMO4, and BLPMO5, whereas those for nano samples were 25.19, 22.25, and 18.14 $m^2\,g^{-1}$, respectively, for nano NLPMO3, NLPMO4, and NLPMO5 samples. A decrease in surface area was noticed with an increase in Pb content both in bulk and nano LPMO perovskite samples. The equivalent spherical diameter of bulk and nano LPMO perovskite samples was

Table 1
Comparison of bond length, bond angle and particle size with characterisation studies.

Studies	Parameters	Sample					
		Bulk			Nano		
		BLPMO3	BLPMO4	BLPMO5	NLPMO3	NLPMO4	NLPMO5
XRD	Mn–O bond Length (μm)	1.959 1.957 1.935	1.944	1.939	1.971	1.965	1.956
XRD	Mn–O–Mn bond angle (°)	162.5 164.5 169.8	179.7	180	179.3	180	180
XRD	Crystallinity size (nm)	340	410	484	35	44	60
BET	Equivalent spherical diameter (nm)	312	399	413	37	43	54
SEM	Particle size (nm)	200–350	400–600	550–800	40–60	55–70	70–90
TEM	Particle size (nm)	300–400	500–650	500–850	47	63	90

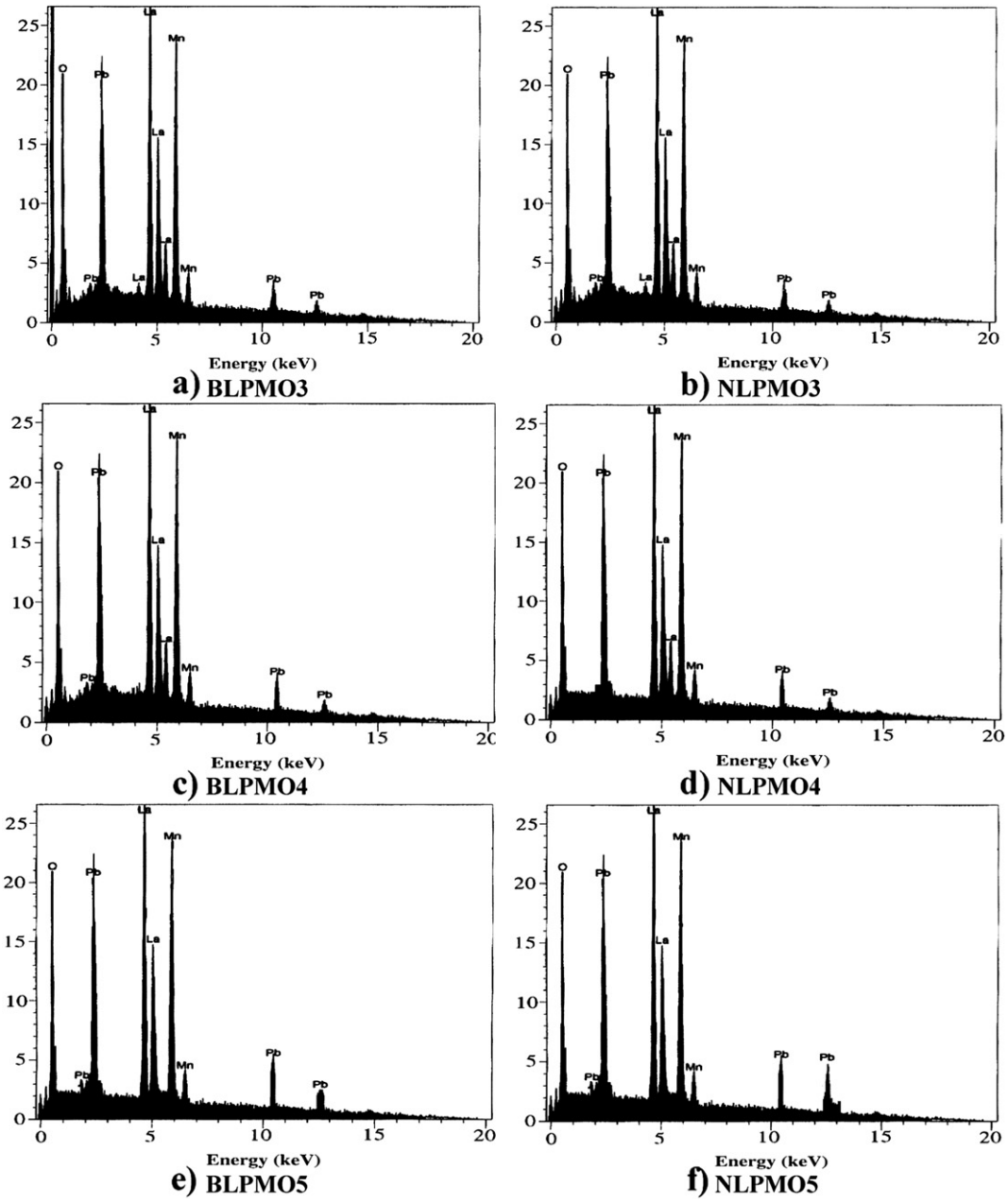

Fig. 2. EDX pattern of bulk $La_{0.7}Pb_{0.3}MnO_3$ (BLPMO3), bulk $La_{0.6}Pb_{0.4}MnO_3$ (BLPMO4), bulk $La_{0.7}Pb_{0.3}MnO_3$ (BLPMO5), nano $La_{0.7}Pb_{0.3}MnO_3$ (NLPMO3), nano $La_{0.6}Pb_{0.4}MnO_3$ (NLPMO4) and nano $La_{0.7}Pb_{0.3}MnO_3$ (NLPMO5) perovskite samples.

obtained using the formula [40] $D_{BET} = 6/\rho S_{BET}$ (where ρ is the density of the sample and S_{BET} is the specific surface area of the sample measured by BET measurement) and is shown in Table 1. The higher surface area of nano LPMO compared with bulk samples denotes that the number of atoms at the surface of nano LPMO samples is more than that of the corresponding bulk samples; that is, large proportions of atoms will either be at or near the grain boundaries of the surface [46,47]. Generally, the increase in surface area and surface free energy leads to a reduction in the interatomic distance for metals; in contrast, the effect is reverse in the case of semiconductors and metal oxides and perovskites [46]. The observed decrease in surface area confirms the increase in interatomic distance; that is, interatomic distance of Mn–O increases with an increase in Pb content. Thus, the observed results from BET studies are in line with those of XRD studies.

Table 2
EDX composition of BLPMO and NLPMO perovskite samples.

Element	Composition from EDX (molar ratio)					
	Bulk			Nano		
	BLPMO3	BLPMO4	BLPMO5	NLPMO3	NLPMO4	NLPMO5
La	0.687	0.601	0.499	0.688	0.584	0.499
Pb	0.291	0.381	0.502	0.289	0.392	0.494
Mn	1.017	0.997	0.990	0.990	0.990	0.998
O	2.999	2.999	2.999	2.999	2.999	2.999

Figs. 4 and 5 (a–f) show the SEM and TEM images of bulk and nano LPMO perovskite samples, respectively. It is evident from the images that particles have spherical-like morphology with fine and clear grain boundaries and narrow range. The range of particle size

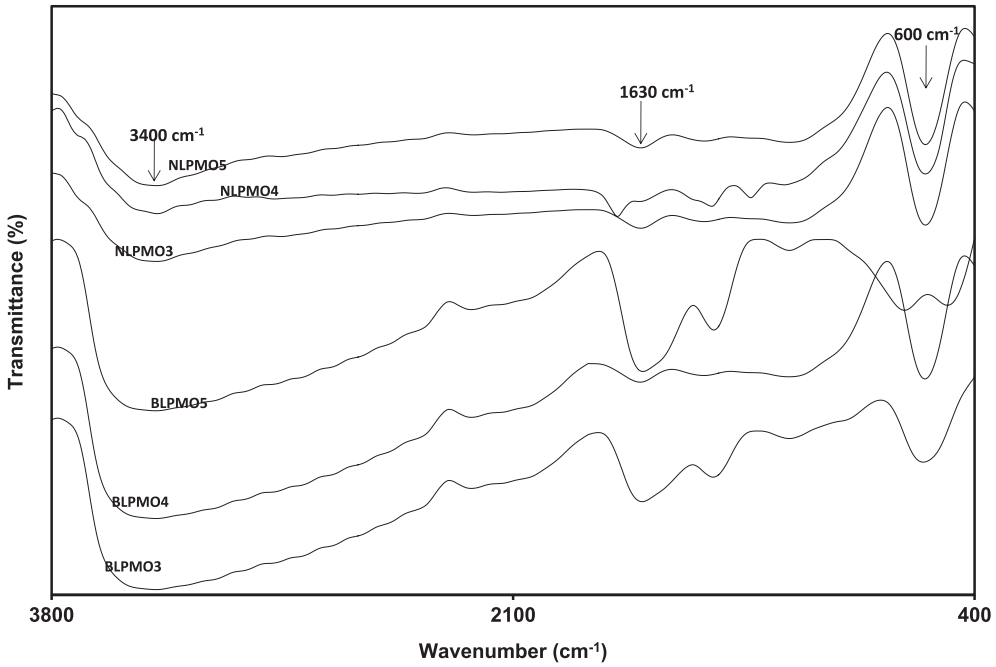

Fig. 3. FTIR spectrum of bulk $La_{0.7}Pb_{0.3}MnO_3$ (BLPMO3), bulk $La_{0.6}Pb_{0.4}MnO_3$ (BLPMO4), bulk $La_{0.7}Pb_{0.3}MnO_3$ (BLPMO5), nano $La_{0.7}Pb_{0.3}MnO_3$ (NLPMO3), nano $La_{0.6}Pb_{0.4}MnO_3$ (NLPMO4) and nano $La_{0.7}Pb_{0.3}MnO_3$ (NLPMO5) perovskite samples.

distribution is obtained considering the minimum and maximum particle size. The estimated particle distribution in bulk and nano LPMO as observed from micrographs (SEM and TEM) is shown in Table 1, along with BET results for comparison. It is evident from Table 1 that the particle size of bulk and nano LPMO perovskites increases with an increase in Pb content from $x = 0.3$ to $x = 0.5$. The range of particle size of bulk and nano LPMO perovskites is confirmed by characterisation studies. The selected area electron diffraction (SAED) of BLPMO and NLPMO perovskite samples is shown in Fig. 5 (inserted). The circular lines in SAED pattern indicate that the BLPMO and NLPMO perovskites are crystalline in nature.

The phase transition temperature of bulk and nano perovskite samples is examined through on-line ultrasonic studies. The ultrasonic velocities and attenuation as a function of temperature have been used to reveal information about the various temperature-dependent phase transitions and its behaviour during the transition both in bulk and nano perovskite samples [34]. The measured density, ultrasonic velocities, attenuations, and the derived elastic moduli at room temperature for both bulk and nano perovskite samples are given in Table 4.

The temperature-dependent longitudinal velocity, shear velocity, longitudinal attenuation, and shear attenuation are shown in Figs. 6–9, respectively. The temperature-dependent ultrasonic parameters show anomalous behaviour both in bulk and nano perovskite manganite samples. The observed anomalous behaviour in ultrasonic measurements as a function of temperature is used to explore the different phase transitions existing in perovskite materials [36]. Most of the solid materials, a monotonic decrease in velocity, and increase in attenuation will be observed as a result of increase in temperature during the absence of any structural/phase transitions [36]. The occurrence of anomalous behaviour, i.e., a dip in velocity or a peak in attenuation, is observed because of the existence of phase/structural transition in materials [35]. The temperature-dependent different phase transitions were identified by correlating the temperature at which an anomalous behaviour is observed in ultrasonic velocities/attenuation with the phase diagram of LPMO perovskites reported from other studies [31–33].

The entire region of temperature (300–400 K) of each sample is divided into three regions, namely, zone I (from 300 K to the temperature at which anomalous behaviour starts, i.e., 353 K for BLPMO3, 357 K for BLPMO4, 358 K for BLPMO5, 340 K for NLPMO3, 344 K for NLPMO4, and 350 K for NLPMO5), zone II (anomalous behaviour zone), and zone III (temperature beyond which anomalous behaviour ends, i.e., 361 K for BLPMO3, 363 K for BLPMO4, 364 K for BLPMO5, 363 K for NLPMO3 and NLPMO4, and 366 K for NLPMO5), for easy discussion of the observed results. The above three zones are clearly represented in Fig. 6 and Table 5. The ultrasonic parameters (Figs. 6–9) show a monotonic behaviour as a function of temperature both in zone I and zone III. However, an anomalous behaviour is observed in zone II. The absence of structural/phase transition in zone I and zone III is confirmed from the observed monotonic decrease in velocities (U_L and U_S) and an increase in attenuations (α_L and α_S). In zone II, the phase transition from FM to PM is revealed from the observed dip in velocities and peak in attenuations by correlating with LPMO phase diagrams [31,32]. Initially in zone II, a fall in velocity up to a critical temperature (transition temperature) followed by an increase in velocity was observed (Figs. 6 and 7). In contrast, the attenuations showed a reverse trend as that of velocity (Figs. 8 and 9). In the BLPMO3 sample in zone II, the sudden fall in velocity started from 353 K and reached a minimum at 357 K, followed by an increase in velocity up to 361 K, whereas in NLPMO3 (in zone II), a fall in velocity started at 340 K and reached a minimum at 352 K, followed by an increase in velocity up to 363 K. It is evident from Table 5 that the minimum in

Table 3
Assignment of functional groups in FTIR spectrum.

Wavenumber (cm^{-1})	Assignment	References
400–600	Mn–O	[44,45]
1630	H–O–H bending mode	[35,44]
3400	O–H stretching vibration	[35,44,45]

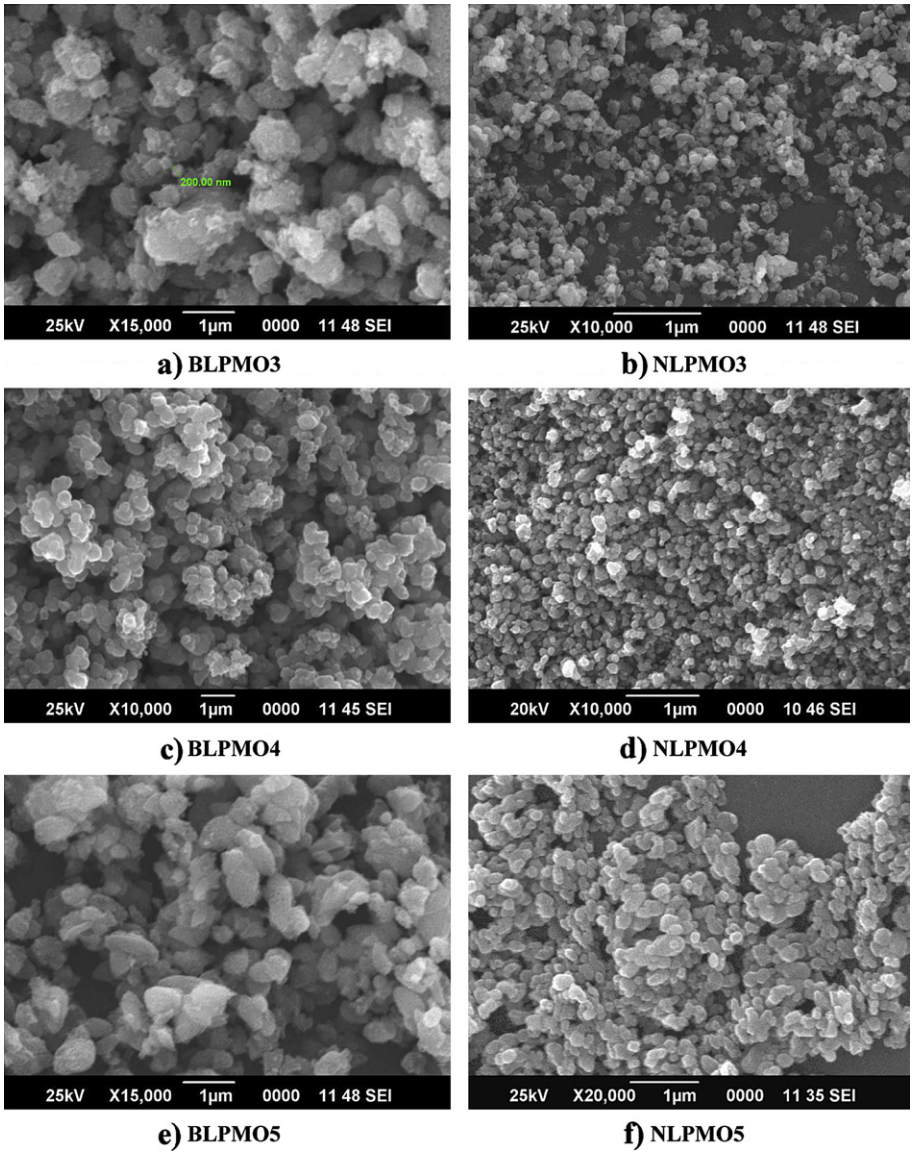

Fig. 4. SEM pattern of bulk $La_{0.7}Pb_{0.3}MnO_3$ (BLPMO3), bulk $La_{0.6}Pb_{0.4}MnO_3$ (BLPMO4), bulk $La_{0.7}Pb_{0.3}MnO_3$ (BLPMO5), nano $La_{0.7}Pb_{0.3}MnO_3$ (NLPMO3), nano $La_{0.6}Pb_{0.4}MnO_3$ (NLPMO4) and nano $La_{0.7}Pb_{0.3}MnO_3$ (NLPMO5) perovskite samples.

sound velocity is shifted to higher temperature with an increase in Pb content from $x = 0.3$ to $x = 0.5$ both in bulk and nano LPMO perovskite samples. A broad dip in velocity/peak in attenuation was noticed in nano perovskite samples compared with bulk samples. The temperature at which a minimum in velocity or a maximum in attenuation is observed is correlated with the phase diagram of LPMO samples [31–33]. The observed anomalous temperature in ultrasonic velocity/attenuation measurements is in agreement with the temperature at which FM–PM phase transition takes place in LPMO perovskite samples [31–33]. Hence, the observed anomalous temperature in zone II was taken as FM–PM phase transition temperature.

The first derivative of longitudinal velocity (Fig. 10) is used to reveal precise information about the temperature-dependent ultrasonic velocity. It shows the predominate peaks used to reveal the precise starting, ending, and anomalous temperature (T_C) of phase transition in zone II. In addition, small ups and down observed around the transition temperature of the prepared samples may be inhomogeneous distribution of Pb or competitions between FM and PM states around the transition temperature [48]. Therefore, the observed minima in velocity at temperatures 357, 360, and 361 K for BLPMO3, BLPMO4, and BLPMO5, respectively, are the FM–PM phase transition temperature (T_C) of the respective samples. Similarly, the phase transition temperature T_C for the NLPMO3, NLPMO4, and NLPMO5 perovskite manganite samples were, respectively, 352, 354, and 358 K. The observed T_C for nano perovskite samples was lower than that for the corresponding bulk perovskite samples. T_C for LPMO perovskites increased with an increase in Pb content, which is qualitatively similar to earlier magnetic studies using a vibrato magnetometer [31].

From Figs. 6–9 it can be seen that bulk LPMO perovskite samples showed a sharp ferromagnetic transition, whereas nano perovskite samples exhibited broad ferromagnetic transition. This is in line with the observation made from the XRD pattern for nanocrystalline samples. To explain the observed behaviour, Curie temperatures (T_C) and transition width (ΔT_C) of all samples were noted and are given in Table 5. It is seen that the broadened transition observed in nano LPMO samples indicate a diffused ferromagnetic

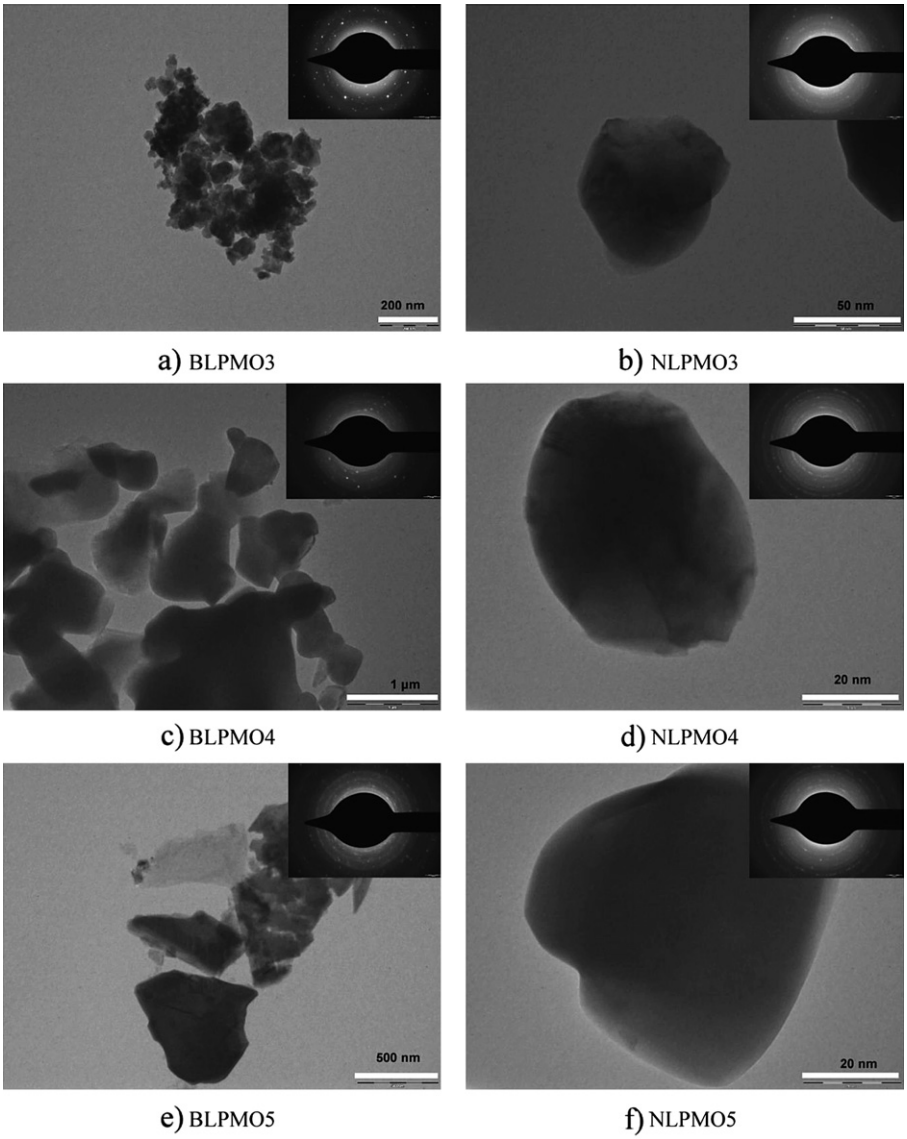

Fig. 5. TEM images of bulk $La_{0.7}Pb_{0.3}MnO_3$ (BLPMO3), bulk $La_{0.6}Pb_{0.4}MnO_3$ (BLPMO4), bulk $La_{0.7}Pb_{0.3}MnO_3$ (BLPMO5), nano $La_{0.7}Pb_{0.3}MnO_3$ (NLPMO3), nano $La_{0.6}Pb_{0.4}MnO_3$ (NLPMO4) and nano $La_{0.7}Pb_{0.3}MnO_3$ (NLPMO5) perovskite samples.

phase transition, i.e., absence of sharp transition. Similar results were reported earlier in case of nanostructured perovskite manganites [35,48]. Further, the observed sharp transitions with a single peak were due to the bulk nature of the sample, which originated from orbitally ordered (OO) phases alone [49]. In contrast, a broad transition with large peaks was considered to be due to the existence of small crystal size attributed to the coexistence of orbitally disordered (OD) and OO phases [49,50].

Table 4
Measured density and ultrasonic parameters at room temperature (300 K).

S. No	Parameters	Bulk			Nano		
		BLPMO3	BLPMO4	BLPMO5	NLPMO3	NLPMO4	NLPMO5
1	Density ($kg\,m^{-3}$)	6503	6345	6216	6436	6271	6126
2	U_L ($m\,s^{-1}$)	4602	4765	4943	4634	4804	4986
3	U_S ($m\,s^{-1}$)	2290	2377	2472	2308	2401	2501
4	α_L ($dB\,cm^{-1}$)	1.98	1.82	1.69	1.97	1.82	1.68
5	α_S ($dB\,cm^{-1}$)	7.67	7.34	7.13	7.49	7.29	7.11
6	L (GPa)	137	144	151	138	145	152
7	G (GPa)	34	36	38	34	36	38
8	K (GPa)	92	96	101	93	97	101
9	E (GPa)	114	120	127	115	121	128
10	Poisson's ratio	0.336	0.334	0.333	0.335	0.334	0.332

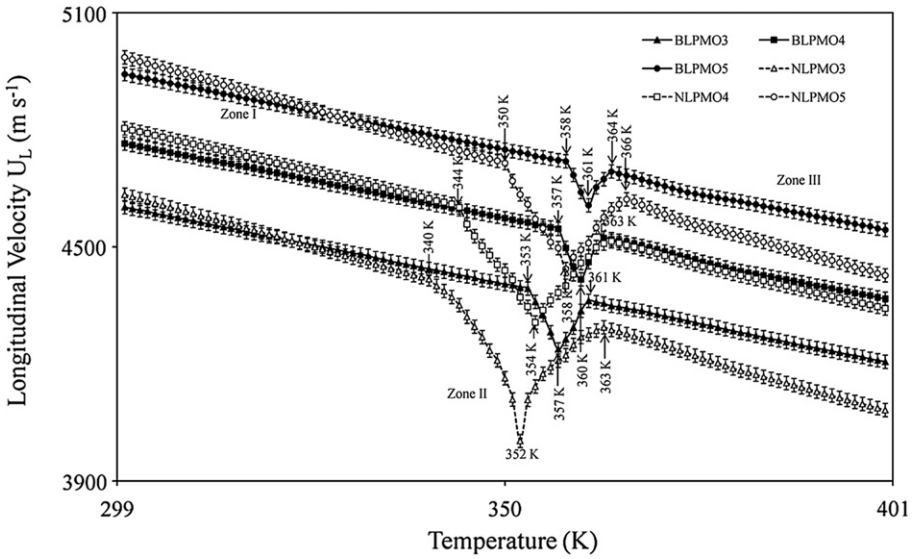

Fig. 6. Temperature dependence of longitudinal velocity of bulk $La_{0.7}Pb_{0.3}MnO_3$ (BLPMO3), bulk $La_{0.6}Pb_{0.4}MnO_3$ (BLPMO4), bulk $La_{0.7}Pb_{0.3}MnO_3$ (BLPMO5), nano $La_{0.7}Pb_{0.3}MnO_3$ (NLPMO3), nano $La_{0.6}Pb_{0.4}MnO_3$ (NLPMO4) and nano $La_{0.7}Pb_{0.3}MnO_3$ (NLPMO5) perovskite samples.

One can directly correlate the occurrence of peak height at transition temperature to lattice softening. Generally, a decrease in velocity and an increase in attenuation are due to the occurrence of lattice softening [34], whereas an increase in velocity and decrease in attenuation are mainly due to lattice hardening [34]. An abrupt change in coupling between spin, charge, orbital, and lattice degrees of freedom and interactions at transition temperature are responsible for the observed anomaly in ultrasonic velocities and attenuations [27,33–36].

It can be observed from Figs. 6–9 that the magnitude of dip in velocity and peak in attenuation in case of nano LPMO perovskites are higher than that of the corresponding bulk perovskite sample. The observed larger magnitude in nano LPMO samples is not only attributed to a conventional FM spin fluctuation near FM–PM transition but is also related to the existence of strong electron–lattice interactions via Jahn–Teller distortion of $Mn^{3+}O_6$ and the spontaneous spin ordering below FM–PM transition [51]. The large softening below T_C in velocities is attributed to the significant change in lattice parameters or the Mn–O bond length [27]. The local distortion of MnO_6 determines the transport properties and CMR properties of perovskite materials. Thus, it leads to a significant reduction in the Jahn–Teller distortion of the $Mn^{3+}O_6$ octahedral because of spin-lattice coupling below the transition temperature [51,52]. This indicates a direct evidence for weak magnetic coupling between the grains below T_C in nano perovskite manganite materials [51,53]. Thus, it leads to low field magnetoresistance in the nanostructured perovskite manganites than in the bulk perovskite samples.

The large change in the magnetic entropy of perovskite manganites could originate from the spin-lattice coupling in the magnetic ordering process [51]. A large magnetic entropy variation in perovskite manganites is interpreted in terms of the double-

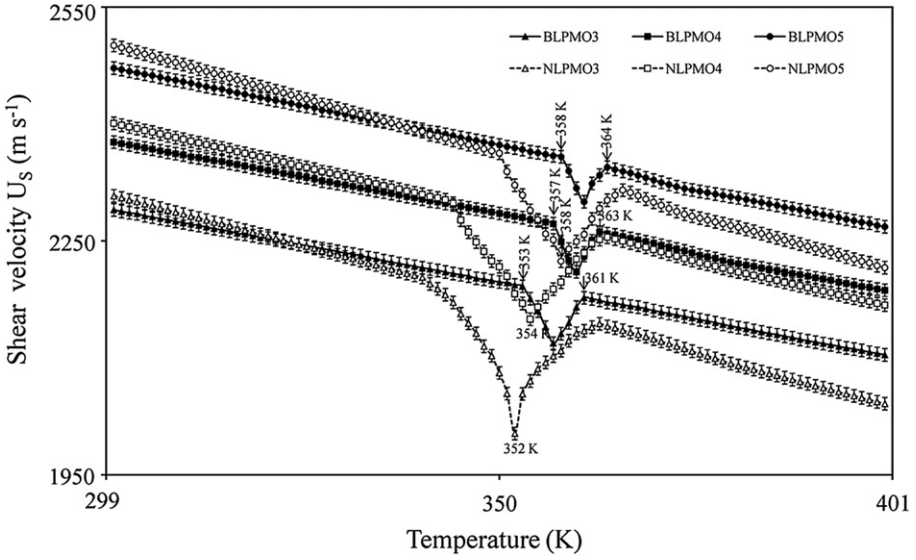

Fig. 7. Temperature dependence of shear velocity of bulk $La_{0.7}Pb_{0.3}MnO_3$ (BLPMO3), bulk $La_{0.6}Pb_{0.4}MnO_3$ (BLPMO4), bulk $La_{0.7}Pb_{0.3}MnO_3$ (BLPMO5), nano $La_{0.7}Pb_{0.3}MnO_3$ (NLPMO3), nano $La_{0.6}Pb_{0.4}MnO_3$ (NLPMO4) and nano $La_{0.7}Pb_{0.3}MnO_3$ (NLPMO5) perovskite samples.

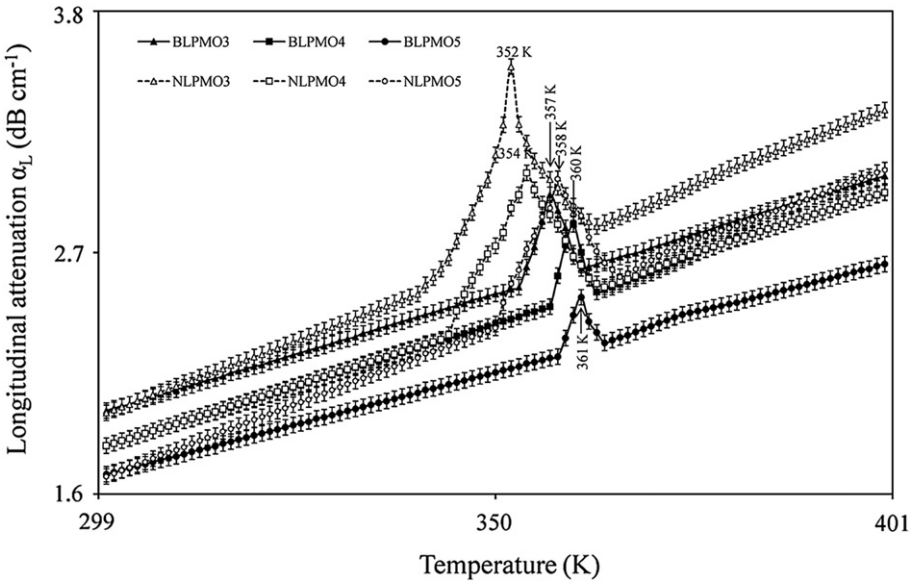

Fig. 8. Temperature dependence of longitudinal attenuation of bulk $La_{0.7}Pb_{0.3}MnO_3$ (BLPMO3), bulk $La_{0.6}Pb_{0.4}MnO_3$ (BLPMO4), bulk $La_{0.7}Pb_{0.3}MnO_3$ (BLPMO5), nano $La_{0.7}Pb_{0.3}MnO_3$ (NLPMO3), nano $La_{0.6}Pb_{0.4}MnO_3$ (NLPMO4) and nano $La_{0.7}Pb_{0.3}MnO_3$ (NLPMO5) perovskite samples.

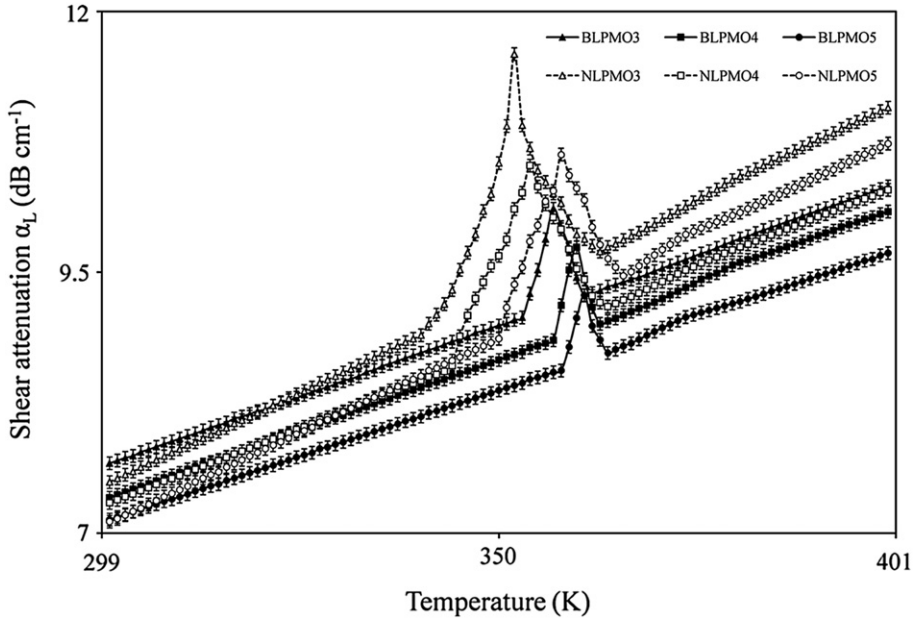

Fig. 9. Temperature dependence of shear attenuation of bulk $La_{0.7}Pb_{0.3}MnO_3$ (BLPMO3), bulk $La_{0.6}Pb_{0.4}MnO_3$ (BLPMO4), bulk $La_{0.7}Pb_{0.3}MnO_3$ (BLPMO5), nano $La_{0.7}Pb_{0.3}MnO_3$ (NLPMO3), nano $La_{0.6}Pb_{0.4}MnO_3$ (NLPMO4) and nano $La_{0.7}Pb_{0.3}MnO_3$ (NLPMO5) perovskite samples.

exchange interaction between Mn^{3+} and Mn^{4+} ions arising from the change in the Mn^{4+}/Mn^{3+} ratio when Pb is doped in $LaMnO_3$ [54]. The observed dip in velocity and peak in attenuation are the direct observation from double-exchange interactions of Mn ions. The width of transition (ΔT_C) in LPMO perovskite samples decreases with an increase in Pb content, which confirms diminishing double-exchange interaction of Mn^{3+}–Mn^{4+} [52,55]. Therefore, the ultrasonic measurements confirm that magnetic entropy decreases with an increase in Pb content.

Further, the observed shift in attenuation peaks towards higher temperatures with an increase in Pb content reveal the changes in relaxation strength which is due to existence of activation energy during the relaxation process of the lattice [56,57]. The decrease in acoustical activation energy (E_p) with increase in Pb content in both BLPMO and NLPMO perovskite samples is confirmed by an increase

Table 5
Temperature range of the region zone I, zone II and zone III of BLPMO and NLPMO perovskite manganite materials.

Zone		Temperature (K)					
		Bulk			Nano		
		BLPMO3	BLPMO4	BLPMO5	NLPMO3	NLPMO4	NLPMO5
I	Start	300	300	300	300	300	300
	End	353	357	358	340	344	350
II	Start	353	357	358	340	344	350
	Anomaly	357	360	361	352	354	358
	End	361	363	364	363	363	366
	Width (ΔT_C)	11	7	7	24	20	17
III	Start	361	363	364	363	363	366
	End	400	400	400	400	400	400

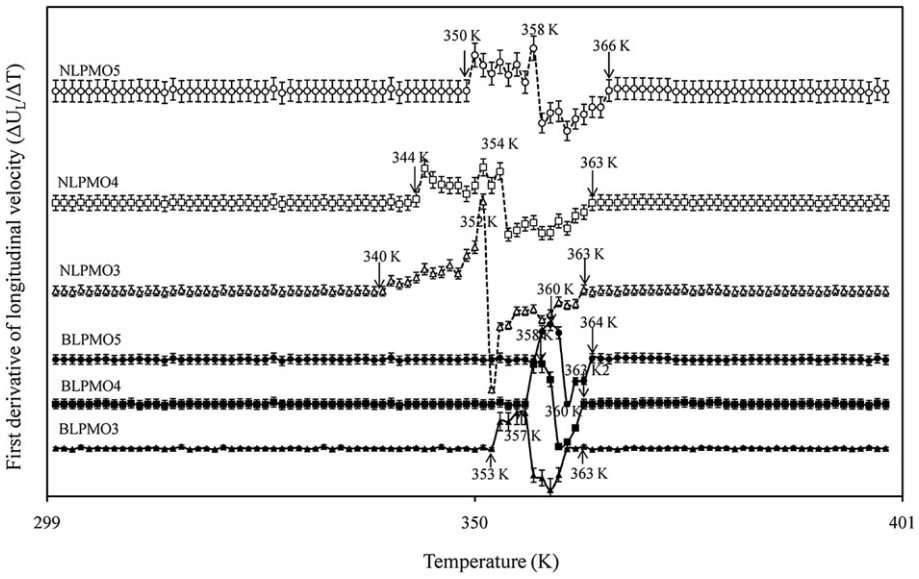

Fig. 10. Temperature dependence of first derivative of longitudinal attenuation of bulk $La_{0.7}Pb_{0.3}MnO_3$ (BLPMO3), bulk $La_{0.6}Pb_{0.4}MnO_3$ (BLPMO4), bulk $La_{0.7}Pb_{0.3}MnO_3$ (BLPMO5), nano $La_{0.7}Pb_{0.3}MnO_3$ (NLPMO3), nano $La_{0.6}Pb_{0.4}MnO_3$ (NLPMO4) and nano $La_{0.7}Pb_{0.3}MnO_3$ (NLPMO5) perovskite samples.

in ultrasonic velocity and a decrease in attenuation with increase in Pb content [56]. The decrease in E_P and thermally activated structural relaxation are responsible for the existence of broad peaks in ultrasonic velocities/attenuation at T_C [56–58].

The existence of a single ion (linear) magnetostriction effect and strong spin–phonon interactions in both bulk and nano lanthanum based perovskite samples is confirmed by the observed anomalous behaviour in both U_L and U_S. Further, the increase in ΔT_C of both BLPMO and NLMPO perovskites (Table 5) is used to reveal the increase in magnetostriction and spin–phonon interactions with the decrease in Pb content in perovskite samples. In case of volume magnetostriction effect, an anomalous behaviour in longitudinal velocity and attenuation exists, whereas shear waves do not show any anomaly [59]. Thus, on-line ultrasonic measurements are more sensitive in exploring the structural/phase transition behaviour in bulk and nano structured perovskite manganite materials.

4. Conclusion

In the present investigation, bulk and nanostructured $La_{1-x}Pb_xMnO_3$ perovskite manganite samples for different Pb contents ($x = 0.30$, 0.40 and 0.50) were synthesised using solid-state reaction and sonochemical methods, respectively. The crystallinity and phase purity of both bulk and nano perovskites were confirmed by XRD. Characterisation studies have confirmed that the particle size of bulk LPMB perovskite samples is in the range of 0.75–85 μm, whereas it ranges from 50 to 90 nm in the case of nano LPMN perovskite samples. Further, it has been confirmed that there is an increase in particle size with an increase in Pb content both in bulk and nano perovskite samples. On-line ultrasonic velocities and attenuation measurements revealed the FM–PM transitions (T_C) at temperatures 357, 360, and 361 K, respectively, for bulk BLPMO3, BLPMO4, and BLPMO5 samples, whereas for nano NLPMO3, NLPMO4, and NLPMO5 samples it took place at 352, 354, and 358 K, respectively. Further, the existence of diffused phase transition in nano LPMO perovskite occurred at lower T_C compared with the corresponding bulk sample, which was revealed from on-line ultrasonic studies. The broad FM–PM transition in nano LPMO perovskites confirms the absence of sharp transition, which is attributed to the coexistence of orbitally ordered and disordered phases. It is evident from the observed anomalies in both velocities and attenuations that the spin–phonon and electron–phonon couplings are known to exist because of single ion magnetostriction and dynamic Jahn–Teller effect, respectively. The above studies confirm that on-line ultrasonic studies are more sensitive in distinguishing bulk and nanostructured perovskite manganite materials on the basis of phase transition temperature.

Ethical statement

I hereby declare that the submitted manuscript has not been published in this or in a similar form and it is not under editorial consideration elsewhere. The article is original, has been written by the stated authors who are all aware of its content and approve its submission, has not been published previously, it is not under consideration for publication elsewhere, no conflict of interest exists, or if such conflict exists, the exact nature of the conflict must be declared and if accepted, the article will not be published elsewhere in the same form, in any language, without the written consent of the publisher.

Acknowledgements

One of the authors (K. S) is thankful to the Council of Scientific and Industrial Research (CSIR), New Delhi (8/570(0001)/2011 dt. 29.03.2011), for Senior Research Fellowship (SRF) to carry out this research project.

References

[1] I. Matos, S. Serio, M.E. Lopes, M.R. Nunes, M.E. Melo Jorge, J. Alloys Compd. 509 (2011) 9617.
[2] C.N.R. Rao, A.P.N. Santosh, A.K. Cheetham, Chem. Mater. 10 (1998) 2714.
[3] R. VonHelmolt, J. Wecker, B. Holzapfel, L. Schultz, K. Samwer, Phys. Rev. Lett. 71 (1993) 2331.
[4] C. Zener, Phys. Rev. Lett. 82 (1951) 403.
[5] A.J. Millis, P.B. Littlewood, B.I. Shraiman, Phys. Rev. Lett. 74 (1995) 5144.
[6] P.-G. de Gennes, Phys. Rev. 118 (1960) 141.
[7] A.J. Campbell, G. Balakrishnan, M.R. Lees, D.McK. Paul, Phys. Rev. B 55 (1997) 8622.
[8] N. Dhahri, A. Dhahri, K. Cherif, J. Dhahri, K. Taibi, E. Dhahri, J. Alloys Compd. 496 (2010) 69.

[9] N. Zhang, W. Ding, W. Zhong, K. Du, K. Wang, Y. Du, Appl. Phys. A 65 (1997) 77.
[10] B. Nadgorny, J. Phys.: B Condens. Matter 19 (2007) 315209.
[11] B. Nadgorny, I.I. Mazin, M. Osofsky, R.J. Soulen Jr., P. Broussard, R.M. Stroud, D.J. Singh, V.G. Harris, A. Arsenov, Ya Mukovskii, Phys. Rev. B 63 (2001) 184433.
[12] Phan Van Cuong, Joonghoe Dho, Hyo Yeol Park, Do-Hyung Kim, Appl. Phys. A 95 (2009) 567.
[13] A. Vailionis, H. Boschker, W. Siemons, E.P. Houwman, D.H.A. Blank, G. Rijnders, G. Koster, Phys. Rev. B 83 (2011) 064101.
[14] Hiroyuki Yamada, Ping-Hua Xiang, Akihito Sawa, Phys. Rev. B 81 (2010) 014410.
[15] E. Arenholz, G. van der Laan, F. Yang, N. Kemik, M.D. Biegalski, H.M. Christen, Y. Takamura, Appl. Phys. Lett. 94 (2009) 072503.
[16] Zhenxing Bi, Emily Weal, Hongmei Luo, Aiping Chen, Judith L. MacManus-Driscoll, Quanxi Jia, Haiyan Wang, J. Phys.: Condes. Matter 109 (2011) 054302.
[17] M. Cantoni, D. Petti, R. Bertacco, I. Pallecchi, D. Marré, G. Colizzi, A. Filippetti, V. Fiorentini, Appl. Phys. Lett. 97 (2010) 032115.
[18] J.R. Chocha, A. Pooja Chhelavda, J.A. Bhalodia, Trans. Ind. Inst. Met. 64 (2011) 159.
[19] C.N.R. Rao, G.U. Kulkarni, P.J.P.P. Thomas Edwards, Chem. A Euro. J. 8 (2002) 28.
[20] Weifan Chen, Jianming Hong, Yongxiu Li, Facile, J. Alloys Compd. 482 (2009) 846.
[21] J. Jeffrey Urban, Wan Soo Yun, Qian Gu, Hongkun Park, J. Am. Chem. Soc. 124 (2002) 1186.
[22] Li Yan, Feiming Bai, Jiefang Li, D. Viehland, J. Am. Ceram. Soc. 92 (2009) 17.
[23] Yasuo Ebina, Takayoshi Sasaki, Masaru Harada, Mamoru Watanabe, Chem. Mater. 14 (2002) 4390.
[24] Xiangyang Ma, Hui Zhang, Jin Xu, Junjie Niu, Qin Yang, Jian Sha, Deren Yang, Chem. Phys. Lett. 363 (2002) 579.
[25] Yuanbing Mao, Sarbajit Banerjee, Stanislaus S. Wong, Chem. Commun. 3 (2003) 408.
[26] D.M. Newns, T. Doderer, C.C. Tsuei, W.M. Donath, J.A. Misewich, A. Gupta, B.M. Grossman, A. Schrott, B.A. Scott, P.C. Pattnaik, J. Electroceram. 4 (2000) 339.
[27] Z. Zhang, Z.C. Li, Q. Jiang, J. Phys. D: Appl. Phys. 33 (2000) 2653.
[28] Ling Zhang, Jifan Hu, Peng Song, Hongwei Qin, Kang An, Xingdong Wang, Minhua Jiang, Sens. Actuators B: Chem. 119 (2006) 315.
[29] Takeshi Egami, Ferroelectrics 222 (1999) 163.
[30] Ling Zhang, Jifan Hu, Peng Song, Hongwei Qin, Xiangdong Liu, Minhua Jiang, Phys. B: Condens. Matter 370 (2005) 259.
[31] Nguyen Chau, Hoang Nam Nhat, Nguyen Hoang Luong, Dang Le Minh, Nguyen Duc Tho, Nguyen Ngoc Chau, Phys. B: Condens. Matter 327 (2003) 270.
[32] Ajay Singh, D.K. Aswal, P. Chowdhury, N. Padma, C.S. Viswanadham, Santosh Kumar, S.K. Gupta, J.V. Yakhmi, J. Magn. Magn. Mater. 313 (2007) 115.
[33] M. Ramesh Babu, X.F. Han, P. Mandal, Ravi Kumar, K. Asokan, R. Jayavel, Mat. Chem. Phys. 117 (2009) 113.
[34] S. Sankarrajan, K. Sakthipandi, V. Rajendran, Phase Transitions 85 (2011) 427.
[35] K. Sakthipandi, V. Rajendran, T. Jayakumar, Baldev Raj, J. Alloys Compd. 509 (2011) 457.
[36] S Sankar rajan, K. Sakthipandi, P. Manivasakan, V. Rajendran, Phase Transitions 84 (2011) 1029.
[37] S. Sankararajan, S. Aravindan, R. Yuvakkumar, K. Sakthipandi, V. Rajendran, J. Magn. Magn. Mater. 321 (2009) 3611.
[38] R.A. Young, The Rietveld Method, Oxford University Press, New York, 1993.
[39] D.B. Wiles, R.A. Young, J. Appl. Cryst. 14 (1981) 149.
[40] B.R. Jennings, K. Parslow, Proc. R. Soc. Lond. A 419 (1988) 137.
[41] P. Palanichamy, P. Kalayanasundram, Baldev Raj, Br. J. Non-dest. Test 31 (1989) 78.
[42] M. Rodriguez-Martinez Lide, Paul Attfield, J. Phys. Rev. B 58 (1998) 2426.
[43] S.S. Rao, S. Tripathi, D. Pandey, S.V. Bhat, Phys. Rev. B 74 (2006) 144416.
[44] Sunita Keshri (Shaw), Leena Joshi, Sanjeeb Kumar Rout, J. Alloys Compd. 485 (2009) 501.
[45] V.S. Kolat, H. Gencer, M. Gunes, S. Atalay, Mat. Sci. Eng. B 140 (2007) 212.
[46] C. Suryanarayana, Adv. Eng. Mater. 7 (2005) 983.
[47] W. Zhong, W. Chen, W.P. Ding, N. Zhang, A. Hu, Y.W. Du, Q.J. Yan, J. Magn. Magn. Mater. 195 (1999) 112.
[48] D.C. Krishna, P. Venugopal Reddy, J. Alloys Compd. 479 (2009) 661.
[49] K. Shantha Shankar, A.K. Raychaudhuri, J. Mater. Res. 21 (2006) 27.
[50] S.V. Trukhanov, A.V. Trukhanov, H. Szymczak, C.E. Botez, A. Adair, J. Low Temp. Phys. 149 (2007) 185.
[51] R.K. Zheng, C.F. Zhu, J.Q. Xie, R.X. Huang, X.G. Li, Mat. Chem. Phys. 75 (2002) 121.
[52] S.G. Min, K.S. Kim, S.C. Yu, H.S. Suh, S.W. Lee, IEEE Trans. Magnet. 41 (2005) 2760.
[53] Sangita Bose, Pratap Raychaudhuri, Rajarshi Banerjee, Parinda Vasa, Pushan Ayyub, Phys. Rev. Lett. 95 (2005) 147003.
[54] T.L. Phan, S.G. Min, M.H. Phan, N.D. Ha, N. Chau, S.C. Yu, Phys. Stat. Sol. (B) 244 (2007) 1109.
[55] S. Jin, T.H. Tiefel, M. McCormack, R.A. Fastnacht, R. Ramesh, L.H. Chen, Science 264 (1994) 413.
[56] Hesham Afifi, Samier Marzouk, Nadia Abd el Aal, Phys. B: Condens. Matter 390 (2007) 65.
[57] G.E. El-Falaky, M.S. Gaafar, N.S. Abd El-Aal, Curr. Appl. Phys. 12 (2012) 589.
[58] Hesham Afifi, Samier Marzouk, Mat. Chem. Phys. 80 (2003) 517.
[59] Changfei Zhu, Renkui Zheng, Phys. Rev. B 59 (1999) 11169.